ISSN 1070-3284, Russian Journal of Coordination Chemistry, 2024, Vol. 50, No. 2, pp. 118–129. © Pleiades Publishing, Ltd., 2024.

Reactions of Carbon Dioxide Bound to Aluminum Diimine Hydride with Borane Dimethyl Sulfide and Ammonia

M. V. Moskalev[a], A. A. Skatova[a, *], A. A. Bazanov[a], E. V. Baranov[a], and I. L. Fedushkin[a]

[a] *Razuvaev Institute of Organometallic Chemistry, Russian Academy of Sciences, Nizhny Novgorod, Russia*

**e-mail: skatova@iomc.ras.ru*

Received May 19, 2023; revised June 6, 2023; accepted June 6, 2023

Abstract—The reaction of aluminum bis-formate acenaphthene-1,2-diimine complex [(Ar^{BIG}-bian)Al(μ-$OC(H)O)_2Li(Thf)_2$] (**I**) (Ar^{BIG}-bian = 1,2-bis[(2,6-dibenzhydryl-4-methylphenyl)imino]acenaphthene), prepared by binding carbon dioxide by aluminum diimine hydride [(Ar^{BIG}-bian)$Al(H)_2]^-[Li(Thf)_4]^+$, with borane dimethyl sulfide and ammonia was studied. The reaction of **I** with $BH_3{\cdot}SMe_2$ (1 : 1) in toluene affords the product of hydroboration of one formate group [(Ar^{BIG}-bian)Al(μ-OC(H)O)$(OB(H)OCH_3)Li(Thf)]_2$ (**II**), while the reaction of **I** with $BH_3{\cdot}SMe_2$ (1 : 2) is accompanied by reduction of both formate groups and gives complex [(Ar^{BIG}-bian)$Al(OBOCH_3)_2OLi_2(Thf)_2BH_4]_2$ (**III**), methoxyboroxine $(CH_3OBO)_3$ and, presumably, compound [(Ar^{BIG}-bian)$AlOCH_3$]. The reaction of **I** with one equivalent of ammonia in THF gives adduct [(Ar^{BIG}-bian)$Al(NH_3)$(μ-$OC(H)O)_2Li(Thf)_2$] (**IV**), in which ammonia is coordinated to the aluminum atom, while the key bonds in **I** have not undergone ammonolysis. Compounds **II**–**IV** were characterized by IR and NMR spectroscopy, elemental analysis, and X-ray diffraction (CCDC no. 2255017 (**II**), 2255018 (**III**), 2255019 (**IV**)).

Keywords: aluminum, hydrides, acenaphthene-1,2-diimines, carbon dioxide, boranes, small molecules, molecular structure

DOI: 10.1134/S1070328423600936

INTRODUCTION

The intensification of modern industrial processes and the increase in the production capacities inevitably lead to higher emission of carbon dioxide to the environment. Since carbon dioxide decreases the Earth's infrared radiation into space at various wavelengths, CO_2 accumulation in the atmosphere enhances the greenhouse effect, increases the Earth's surface temperature and, as a consequence, increases the risks of some environmental and socio-economic problems [1]. Meanwhile, the CO_2 molecule can be considered as a renewable source of carbon and an available C_1-synthon for chemical industry. This fact attracts particular attention of researchers and stimulates the search for methods of capturing, binding and catalytic transformation of carbon dioxide into practically valuable chemicals, in particular hydrocarbons, ethanol, cyclic carbonates, and some other [2–7]. The CO_2 conversion is often performed using homogeneous catalytic systems containing transition metals [2–4, 6]. However, in recent years, there has been considerable interest in the use of main group metal complexes as catalysts for reactions involving carbon dioxide as inexpensive, readily available and low-toxicity alternatives to *d*-element derivatives. In particular, aluminum scorpionate [8], indene [9], guanidinate [10], and amidinate [11] derivatives have shown high activity towards the catalytic addition of CO_2 to alkene oxides. One more example of effective use of main group metal complexes in the functionalization of carbon dioxide is hydrogenation by silicon and organoboron compounds. For example, magnesium [12, 13], aluminum [14], and gallium [15] compounds activated with tris(pentafluorophenyl)borane $B(C_6F_5)_3$ can perform catalytic hydrosilylation of CO_2 to bis-silylacetal and methoxysilyl derivatives and methane. Using magnesium tris[(1-isopropylbenzimidazol-2-yl)dimethylsilyl]methyl complex {[$Tism^{iPrBenz}$]Mg}[$HB(C_6F_5)_3$], carbon dioxide and triphenylsilane were converted to bis-silylacetal $H_2C(OSiPh_3)_2$, which is a source of formaldehyde monomer and the CH_2 group able to

functionalize various classes of organic compounds [13]. Hydrogenation reactions of CO_2 by various boranes in the presence of catalytic amounts of main group metal complexes are also known. In particular, magnesium, calcium [16], aluminum [17], and gallium [18] β-diketiminate hydride derivatives successfully catalyze the hydroboration of carbon dioxide with pinacolborane (HBpin) to give methanol precursor, methoxyboronic acid pinacol ester ($pinBOCH_3$). In addition, studies of the catalytic activity of aluminum bis-imidazole [19] and bis(phosphoranyl)methanide [20] hydrides in the reactions of CO_2 with some boranes demonstrated that the borohydride structure (pinacolborane, catecholborane, $BH_3{\cdot}SMe_2$) influences the selectivity and the yield of reduction products. As a rule, in all of the above examples of hydroboration and hydrosilylation using hydride complexes, the catalytic cycle is triggered by insertion of CO_2 molecule into the metal–hydrogen bond of the complex. In some cases, the resulting formate derivatives have been isolated and characterized. These products are capable of subsequent successive hydrogenation and formation of acetal or methoxy products and generation of catalytically active metal hydride intermediates, which react with the next CO_2 molecule [12, 13, 15, 16, 18–20]. However, both the formation of the formate derivative and its subsequent reduction are not sufficient conditions for implementation of the catalytic cycle of carbon dioxide transformation. For example, despite the ability of the aluminum β-diketiminate hydride complex (NacNac)Al(Et)H (NacNac = $C(MeC^{Dpp}N)_2$, Dpp = 2,6-^{i}Pr–C_6H_3) to form the formate (NacNac)Al(Et)OCHO in the reaction with CO_2, the reduction of the formate with various borohydrides does not lead to regeneration of the initial aluminum hydride or other molecular system containing an active Al–H bond [21]. Instead, aluminum boroxyl complexes unable to bind carbon dioxide molecules are formed; this rules out the use of compound (NacNac)Al(Et)H as a catalyst. Hence, a detailed study of stoichiometric reactions of carbon dioxide with main group metal hydride complexes and reduction of the resulting adducts is an important task.

Previously, we synthesized various aluminum dihydride derivatives based on acenaphthene-1,2-diimine ligands Dpp-bian and Ar^{BIG}-bian (Dpp-bian = 1,2-bis[(2,6-diisopropylphenyl)imino]acenaphthene; Ar^{BIG}-bian = 1,2-bis[(2,6-dibenzhydryl-4-methylphenyl)imino]acenaphthene) [22–24] (Scheme 1).

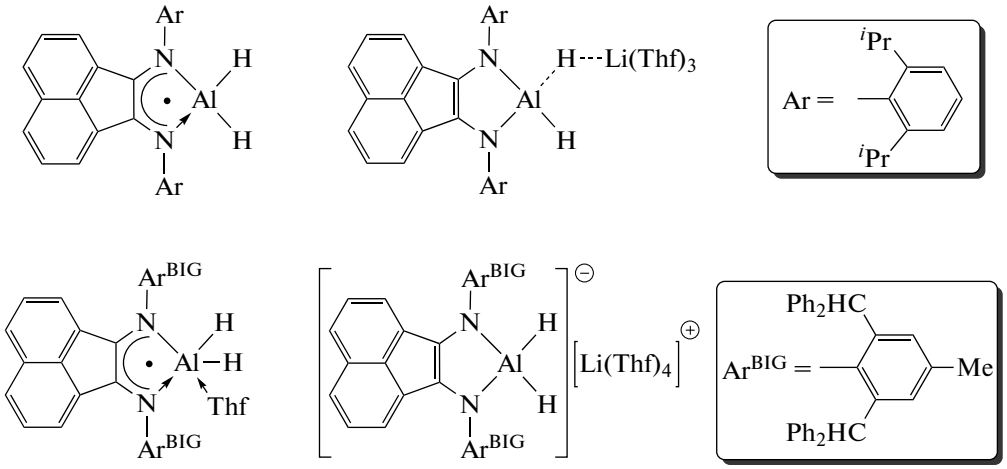

Scheme 1.

The reactions of these dihydrides with carbon dioxide demonstrated the effect of ligand steric crowding on the structure of hydroalumination products and on the reaction selectivity [24, 25]. In addition, hydroboronation of gem-diolate [{(Dpp-bian)AlO_2CH_2}$_2$] [26, 27] and bis-formate [(Ar^{BIG}-bian)Al(μ-OC(H)O)$_2$Li(Thf)$_2$] [26] (**I**) derivatives by some boranes has been studied. Quantum chemical calculations for the reduction of [{(Dpp-bian)AlO_2CH_2}$_2$] were carried out, and the relationship between the structure of the borohydride used and the preferred reactions pathway was established [26, 27]. In continuation of studies of the appli-

cability of aluminum hydride derivatives based on Ar-bian ligands for CO_2 transformation, here we studied the reactions of bis-formate **I** with borane dimethyl sulfide ($BH_3{\cdot}SMe_2$) in 1 : 1 and 1 : 2 molar ratios. Derivative **I** was chosen because of the ease of its preparation in high yield by the reaction of the corresponding dihydride with a stoichiometric amount of CO_2, and the $BH_3{\cdot}SMe_2$ hydroboration agent was chosen due to its ready availability and common use as a reducing agent for unsaturated compounds, including carbonyl compounds. We also carried out the reaction of **I** with ammonia to determine the applicability of **I** for reductive hydroformylation of amines. This reaction is especially popular because it provides the methylation of amines with carbon dioxide in the presence of reducing agents, such as silanes, without the use of potentially hazardous reagents such as methyl iodide and diazomethane [28–31].

EXPERIMENTAL

All operations involved in the synthesis, isolation, and identification of the complexes were performed in vacuum using the Schlenk technique or argon atmosphere (Glovebox M. Braun). Bis-formate **I** was obtained by the reaction of the dihydride [(Ar^{BIG}-bian)Al(H)$_2$]$^-$[Li(Thf)$_4$]$^+$ [25] with excess CO_2. Borane dimethyl sulfide (Aldrich) was used as received. Ammonia (99.9999%, Horst) was withdrawn from a cylinder into a tube using a vacuum gas line without preliminary purification/drying. Tetrahydrofuran, deuterotetrahydrofuran, and toluene were dried by refluxing over sodium benzophenone ketyl, stored in an inert atmosphere over molecular sieves (3 Å), and withdrawn in a nitrogen flow immediately before use. IR spectra were recorded on an FSM-1201 spectrometer. ^{1}H, ^{7}Li, ^{11}B, ^{13}C, and HSQC NMR spectra were recorded on Bruker Avance NEO 300 (300 MHz) and Bruker Avance III (400 MHz) spectrometers. Elemental analysis was performed by combustion of samples in an Elementar Vario EL Cube automatic analyzer. The yields of the synthesized complexes were calculated in relation to the amount of (Ar^{BIG}-bian)Al(H)$_2$]$^-$[Li(Thf)$_4$]$^+$ used.

Synthesis of [(Ar^{BIG}-bian)Al(μ-OC(H)O)(OB(H)-OCH$_3$)Li(Thf)]$_2$ (II). From the dark blue solution of compound **I** (0.5 mmol, 0.86 g) obtained in situ in THF (20 mL), THF was removed under reduced pressure, and toluene (15 mL) was added. Then borane dimethyl sulfide $BH_3{\cdot}SMe_2$ (0.038 g, 0.5 mmol) was added to the resulting solution by condensation. Crystallization of the solution gave blue rhombohedral crystals of **II**$\cdot 4C_6H_5CH_3$. The yield was 0.39 g (55%). T_m = 220–225°C (dec.).

IR (ν, cm^{-1}): 3084 w, 3057 w, 3025 w, 1613 vs (OC(H)O), 1515 m, 1493 s, 1445 s, 1335 w, 1318 m, 1293 w, 1275 m, 1179 m, 1155 w, 1128 w, 1077 m, 1052 w, 1032 s, 1003 w, 979 m, 932 s, 915 m, 856 m, 830 m, 809 w, 760 s, 742 m, 701 vs, 677 s, 645 w, 623 m, 605 s, 578 w, 562 m.

^{1}H NMR (300 MHz; THF-d$_8$; 298 K; δ, ppm, *J*/Hz) 7.26–6.90 (m, 72H, arom. and 20H, $C_6\underline{H}_5CH_3$), 6.78–6.65 (m, 16H, arom. and 4H, $C\underline{H}(Ph)_2$), 6.62 (d, 4H, naphthalene moiety, J = 8.08), 6.55 (s, 4H, $C\underline{H}(Ph)_2$), 6.36 (s., 2H, $OC(\underline{H})O$), 6.11 (dd, 4H, naphthalene moiety, J_1 = 7.03, J_2 = 8.08), 4.87 (d, 4H, naphthalene moiety, J = 7.03), 3.99 (br.s, 2H, B$\underline{H}$), 3.59 (s, 16H, THF), 2.78 (s, 6H, $OC\underline{H}_3$), 2.32 (s, 12H, $C_6H_5C\underline{H}_3$), 2.23 (s, 12H, $C\underline{H}_3$), 1.74 (s, 16H, THF).

For $C_{196}H_{178}B_2N_4O_{10}Li_2Al_2$ (M = 2838.87)			
Anal. calcd., %	C, 82.92	H, 6.32	N, 1.97
Found, %	C, 82.53	H, 6.38	N 2.04

Synthesis of [(Ar^{BIG}-bian)Al(OBOCH$_3$)$_2$OLi$_2$-(Thf)$_2$BH$_4$]$_2$ (III). From the dark blue solution of compound **I** (0.5 mmol, 0.86 g) obtained in situ in THF (20 mL), THF was removed under reduced pressure, and toluene (15 mL) was added. Then borane dimethyl sulfide $BH_3{\cdot}SMe_2$ (0.076 g, 1.0 mmol) was added to the resulting solution by condensation. The solution color did not change. Crystallization from the solution gave green plate crystals of **III**$\cdot 2C_6H_5CH_3$. The yield was 0.26 g (36%). T_m = 192–195°C (dec.).

IR (ν, cm^{-1}): 3083 w, 3058 w, 3026 w, 2308 (B–H) s, 2244 (B–H) s, 1621 s, 1599 s, 1539 w, 1530 w, 1504 vs, 1493 vs, 1439 vs, 1333 s, 1289 w, 1274 m, 1217 m, 1197 w, 1156 w, 1145 w, 1129 m, 1102 s, 1077 m, 1031 s, 1002 w, 978 w, 954 w, 931 vs, 893 s, 881 s, 852 w, 807 m, 800 w, 788 w, 760 vs, 743 m, 728 m, 698 vs, 623 s, 607 s.

^{1}H NMR (400 MHz; THF-d$_8$; 297.1 K; δ, ppm, *J*/Hz): 7.23–7.17 (m, 8H, arom.), 7.17–7.05 (m, 24H, arom. and 20H, $C_6\underline{H}_5CH_3$), 7.05–6.95 (m, 24H, arom.), 6.89 (s, 8H, C$\underline{H}$ *meta*-Ar^N), 6.85 (s, 8H, $C\underline{H}(Ph)_2$), 6.65–6.56 (m, 24H, arom.), 6.42 (d, 4H, naphthalene moiety, J = 8.03), 5.99 (dd, 4H, naphthalene moiety, J_1 = 7.03, J_2 = 8.03), 4.81 (d, 4H, naphthalene moiety, J = 7.03), 3.60 (s, 32H, THF), 2.78 (s, 12H, $OC\underline{H}_3$), 2.32 (s, 12H, $C_6H_5C\underline{H}_3$), 2.20 (s, 12H, $C\underline{H}_3$), 1.74 (s, 32H, THF), –0.47 (sept. and quart., 8H, $^{10,11}B\underline{H}_4$, J_1 = 27.10, J_2 = 81.19). ^{7}Li NMR

(155 MHz, THF-d_8, 297.1 K): –0.75 (s). $^{11}B\{^1H\}$ NMR (128 MHz, THF-d_8, 297.1 K): –41.76 (s).

For $C_{190}H_{188}B_6N_4O_{14}Li_4Al_2$ (M = 2898.01)			
Anal. calcd., %	C, 78.74	H, 6.54	N, 1.93
Found, %	C, 78.93	H, 6.47	N, 2.01

Synthesis of [(Ar^{BIG}-bian)Al(NH_3)(μ-OC(H)O)$_2$-Li(Ehf)$_2$] (IV). Ammonia (0.51 mmol, 12.3 mL) was condensed into a frozen dark brown solution of compound **I**, obtained in situ by the action of excess CO_2 on a solution of dihydride ([(Ar^{BIG}-bian)Al$(H)_2]^-$[Li$(Thf)_4]^+$ (0.5 mmol, 0.86 g) in THF (20 mL). As the reaction mixture was slowly heated to room temperature, the color of the solution changed from dark blue to green. Crystallization from the solution gave green rhombohedral crystals of **IV**·2Thf. The yield was 0.51 mg (70%). T_m = 158–160°C (dec.).

IR (ν, cm^{-1}): 3347 m (N–H), 3267 w, 3082 w, 3057 w, 3024 w, 1654 (OC(H)O) vs, 1600 s, 1527 vs, 1494 s, 1351 s, 1290 w, 1269 m, 1214 w, 1181 s, 1153 w, 1069 s, 1048 m, 1032 m, 1003 m, 930 s, 917 w, 893 w, 832 w, 807 m, 797 w, 755 s, 701 vs, 683 w, 659 m, 622 m, 606 s, 566 m.

^1H NMR (400 MHz, C_6D_6, 298.4 K, δ, ppm, J/Hz): 7.25–7.15 (m, 18H, arom. and 2H, naphthalene moiety), 6.97–6.89 (m, 10H, arom.), 6.89–6.88 (m, 16H, arom.), 6.71 (s, 2H, OC(H)O), 6.71 (dd, 2H, naphthalene moiety, J_1 = 8.28, J_2 = 7.03), 6.63 (s, 4H, CH(Ph)$_2$), 6.14 (d, 2H, naphthalene moiety, J = 7.03), 1.95 (s, 6H, CH_3), 0.97 (br.s., 3H, NH_3). ^{15}N NMR (based on ^1H–^{15}N HSQC NMR, 40.55 MHz, C_6D_6, 298.4 K, δ, ppm): 11.5.

For $C_{96}H_{97}N_3O_8LiAl$ (M = 1454.68)			
Anal. calcd., %	C, 79.26	H, 6.72	N, 2.89
Found, %	C, 78.62	H, 6.94	N, 2.49

X-ray diffraction study of **II**·4$C_6H_5CH_3$, **III**·2$C_6H_5CH_3$ and **IV**·2Thf (below referred to as **II**, **III**, **IV** for simplicity) was carried out on a Bruker D8 Quest three-circle automated diffractometer (ω- and φ-scan modes, MoK_α radiation, λ = 0.71073 Å, T = 100(2) K). X-ray diffraction data collection, initial reflection indexing, and refinement of unit cell parameters were carried out using the APEX3 program [32]. Experimental sets of intensities were integrated using the SAINT program [33, 34]. The structures were solved by the dual-space method with the SHELXT program [35] and refined by the full-matrix least squares method on F^2_{hkl} in the anisotropic approximation for non-hydrogen atoms. The hydrogen atoms were placed into geometrically calculated positions and refined isotropically in the riding model. The hydrogen atoms of the OC(H)O formate ligands and OB(H)O moieties in **II** and borohydride groups BH_4 in **III** were found from difference Fourier maps and refined isotropically. The structure refinements were carried out using the SHELXTL program package [36, 37]. The absorption corrections were applied by the SADABS program [38]. In the crystals of **II**, **III**, and **IV**, toluene (**II**, **III**) and THF (**IV**) solvent molecules disordered in the general position were found in 4 : 1, 2 : 1, and 2 : 1 ratios to the Al complex molecule, respectively. In complex **III**, the coordinated THF molecules are disordered over two sites. Similarly, in complex **IV**, one Ph substituent of the Ar^{BIG}-bian ligand is disordered over two sites. Crystallographic data and X-ray diffraction experiment details are summarized in Table 1; selected bond lengths and bond angles are in Tables 2, 3, and 4 for compounds **II**, **III**, and **IV**, respectively.

The crystal structure parameters are deposited with the Cambridge Crystallographic Data Centre (CCDC nos. 2255017 (**II**), 2255018 (**III**), 2255019 (**IV**), ccdc.cam.ac.uk/getstructures).

RESULTS AND DISCUSSION

One molar equivalent of BH_3·SMe_2 was added to a solution of compound **I** in toluene by vacuum condensation. Blue rhombohedral crystals of the hydroboration product [(Ar^{BIG}-bian)Al(μ-OC(H)O)(OB(H)-OCH_3)Li(Thf)]$_2$ (**II**) were isolated by crystallization (~24 h) from the reaction mixture in 55% yield (Scheme 2). The product was characterized by IR and NMR spectroscopy, elemental analysis, and X-ray diffraction.

The reaction proceeds as selective hydroboration of one of the formate groups in **I** to form the $OB(H)OCH_3$ moiety and gives dimer **II** due to binding of lithium atoms by carbonyl oxygen atoms. We suggest that the formate ion reduction proceeds via the intermediate formation of acetal containing an Al–O–CH_2–O–BH_2 unit. This is followed by intramolecular rearrangement to give an Al–O–BH_2 moiety and lithium atom-coordinated formaldehyde molecule. Formaldehyde is hydroborated at the C=O bond to afford the Al–$OB(H)OCH_3$ moiety. A similar mechanism was proposed for the formation of (NacNac)Al(Et)$OB(H)OCH_3$ by the reaction of aluminum diketiminate complex (NacNac)Al(Et)-OCHO with BH_3·SMe_2 [21].

Table 1. Crystallographic data and X-ray experiment and structure refinement details for **II**·$4C_6H_5CH_3$, **III**·$2C_6H_5CH_3$, and **IV**·2Thf

Parameters	Values		
	II·$4C_6H_5CH_3$	**III**·$2C_6H_5CH_3$	**IV**·2Thf
Molecular formula	$C_{196}H_{178}B_2N_4O_{10}Li_2Al_2$	$C_{190}H_{188}B_6N_4O_{14}Li_4Al_2$	$C_{96}H_{97}N_3O_8LiAl$
M	2838.87	2898.01	1454.68
System	Triclinic	Monoclinic	Orthorhombic
Space group	$P\bar{1}$	$P2_1/n$	$Pbca$
Temperature, K	100(2)	100(2)	100(2)
a, Å	15.3731(8)	14.8500(6)	21.8482(7)
b, Å	15.6121(8)	20.6609(9)	26.3438(9)
c, Å	18.1505(9)	27.0145(11)	28.0759(9)
α, deg	65.077(2)	90	90
β, deg	82.665(2)	104.5012(13)	90
γ, deg	75.969(2)	90	90
V, Å^3	3831.1(3)	8024.4(6)	16159.5(9)
Z	1	2	8
ρ(calcd.), g/cm^3	1.230	1.199	1.196
μ, mm^{-1}	0.085	0.083	0.085
F(000)	1504	3072	6192
Crystal size, mm	0.27 × 0.17 × 0.09	0.32 × 0.19 × 0.16	0.42 × 0.13 × 0.07
Measurement range of θ, deg	2.21–27.21	2.03–26.02	1.71–26.02
Ranges of reflection indices	$-19 \le h \le 19$, $-20 \le k \le 20$, $-23 \le l \le 23$	$-18 \le h \le 18$, $-25 \le k \le 25$, $-33 \le l \le 33$	$-26 \le h \le 26$, $-32 \le k \le 31$, $-32 \le l \le 34$
Number of measured reflections	166326	101571	159880
Number of unique reflections (R_{int})	16758 (0.0628)	15809 (0.0565)	15905 (0.1045)
Number of reflections with $I > 2\sigma(I)$	12743	12837	10733
Absorption correction (max/min)	0.959/0.837	0.9586/0.8004	0.746/0.613
Data/constraints/parameters	16758/1223/1069	15809/230/1036	15905/1159/1025
GOOF	1.062	1.075	1.040
R_1, wR_2 ($I > 2\sigma(I)$)	0.0656/0.1342	0.0993/0.2214	0.0877/0.2365
R_1, wR_2 (for all reflections)	0.0926/0.1464	0.1198/0.2316	0.1271/0.2624
$\Delta\rho_{max}/\Delta\rho_{min}$, e Å^{-3}	0.603/–0.469	0.626/–1.088	1.158/–0.594

Table 2. Selected bond lengths and angles in complex **II**·4$C_6H_5CH_3$

Bond	*d*, Å	Bond	*d*, Å
Al(1)–N(1)	1.8319(18)		
Al(1)–N(2)	1.8443(17)	O(1)–C(79)	1.272(3)
Al(1)–O(1)	1.7972(17)	O(2)–C(79)	1.218(3)
Al(1)–O(3)	1.7414(16)	O(3)–B(1)	1.347(3)
Li(1)–O(2)	1.937(5)	O(4)–B(1)	1.353(3)
O(2)–Li(1)'	2.015(5)	N(1)–C(1)	1.411(3)
Li(1)–O(3)	2.013(5)	N(2)–C(2)	1.402(3)
Li(1)–O(4)	2.318(6)	C(1)–C(2)	1.375(3)
Angle	ω, deg	Angle	ω, deg
N(1)Al(1)N(2)	93.09(8)	O(2)Li(1)O(3)	96.9(2)
O(1)Al(1)O(3)	103.07(8)	O(2)'Li(1)O(4)	100.6(2)
O(3)Li(1)O(4)	62.78(15)	Li(1)O(2)Li(1)'	96.03(19)
O(2)Li(1)O(2)'	83.97(19)		

Table 3. Selected bond lengths and angles in complex **III**·2$C_6H_5CH_3$

Bond	*d*, Å	Bond	*d*, Å
Al(1)–N(1)	1.842(3)	Li(2)–H(2)	2.13(5)
Al(1)–N(2)	1.842(3)	Li(2)–H(3)'	1.93(5)
Al(1)–O(1)	1.772(3)	O(1)–B(2)	1.315(5)
Al(1)–O(2)	1.756(3)	O(2)–B(3)	1.329(5)
Li(1)–O(3)	1.946(9)	O(4)–B(2)	1.403(5)
Li(1)–O(4)	2.092(8)	O(4)–B(3)	1.398(5)
Li(2)–O(5)	1.952(8)	N(1)–C(1)	1.406(5)
Li(1)–H(1)	1.90(6)	N(2)–C(2)	1.400(4)
Li(1)–H(2)	1.88(5)	C(1)–C(2)	1.373(5)
Angle	ω, deg	Angle	ω, deg
N(1)Li(1)N(2)	92.95(14)	O(3)Li(1)O(4)	68.0(3)
O(1)Al(1)O(2)	99.94(13)	H(1)Li(1)H(2)	57(3)
Al(1)O(1)B(2)	123.3(3)	O(4)Li(1)H(2)	99.4(16)
Al(1)O(2)B(3)	125.4(3)	O(3)Li(1)H(1)	99(2)
O(1)B(2)O(4)	126.0(4)	O(5)Li(2)H(3)'	95(2)
O(2)B(3)O(4)	123.2(4)	H(3)'Li(2)H(2)	136(2)
B(2)O(4)B(3)	121.7(3)	H(2)Li(2)O(5)	118.3(15)

Table 4. Selected bond lengths and angles in complex **IV**·2Thf

Bond	*d*, Å	Bond	*d*, Å
Al(1)–N(1)	1.897(3)	Li(1)–O(6)	1.942(8)
Al(1)–N(2)	1.918(3)	O(1)–C(79)	1.283(4)
Al(1)–N(3)	2.049(3)	O(2)–C(79)	1.218(4)
Al(1)–O(1)	1.833(3)	O(3)–C(80)	1.260(4)
Al(1)–O(3)	1.836(3)	O(4)–C(80)	1.219(5)
Li(1)–O(2)	1.841(8)	N(1)–C(1)	1.410(4)
Li(1)–O(4)	1.881(8)	N(2)–C(2)	1.379(4)
Li(1)–O(5)	1.963(8)	C(1)–C(2)	1.383(5)
Angle	ω, deg	Angle	ω, deg
N(1)Al(1)N(2)	86.18(12)	Al(1)O(3)C(80)	150.1(3)
N(2)Al(1)N(3)	169.99(13)	O(1)C(79)O(2)	127.7(4)
N(1)Al(1)N(3)	89.43(12)	O(3)C(80)O(4)	127.0(4)
O(1)Al(1)O(3)	111.40(12)	C(79)O(2)Li(1)	145.7(3)
O(1)Al(1)N(1)	110.92(12)	C(80)O(4)Li(1)	140.5(4)
O(3)Al(1)N(1)	137.57(13)	O(2)Li(1)O(4)	115.0(4)
Al(1)O(1)C(79)	141.0(2)	O(5)Li(1)O(6)	113.7(4)

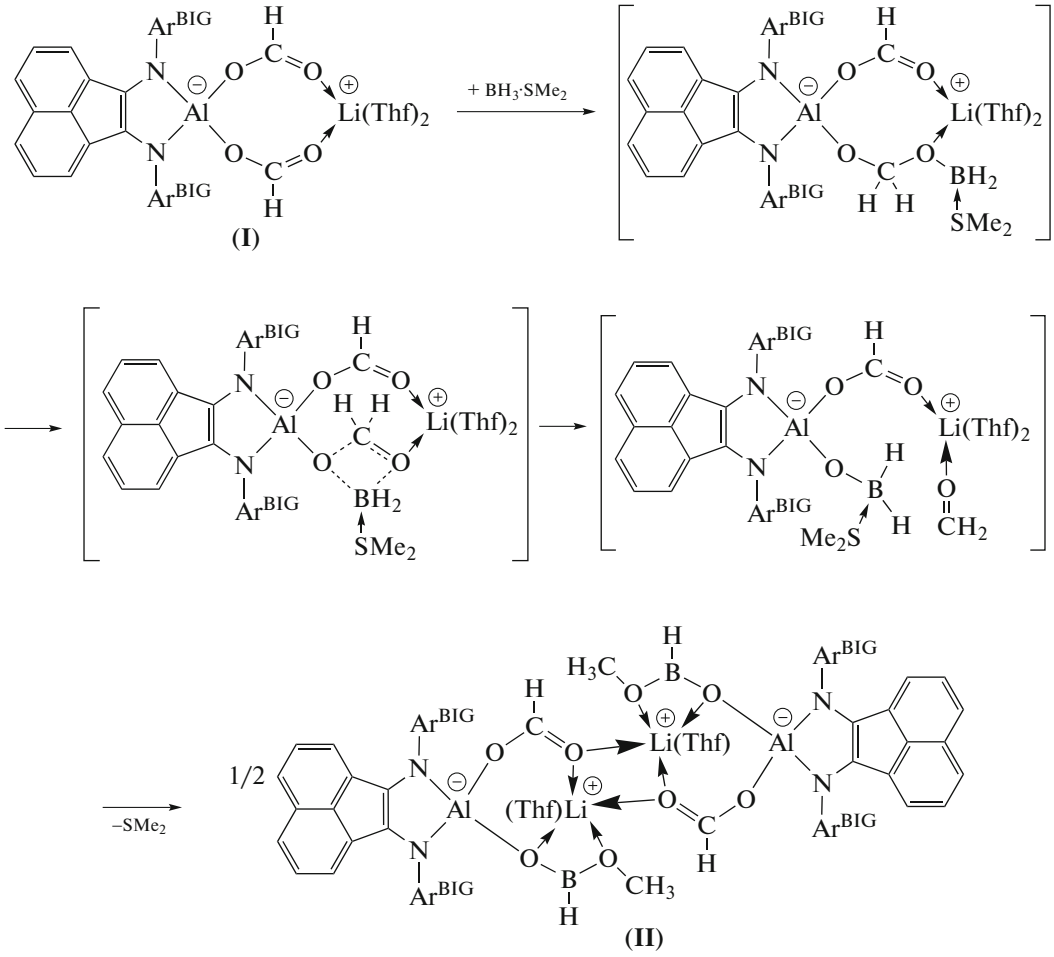

Scheme 2.

From the data of NMR (^{1}H, DEPT, ^{1}H–^{13}C HSQC) spectroscopy, the proton and carbon chemical shifts for the key units of **II** were determined. The $-OCH_3$ and $-OC(H)O-$ substituents are characterized by δ_H 2.78 (s, 6H) and δ_C 51.0 (2C) ppm and also δ_H 6.36 (s, 2H) and δ_C 165.8 (2C) ppm, respectively. Hydride ions bound to boron atoms appear as broadened singlets at δ_H 3.99 ppm (2H). Unfortunately, we were unable to record the ^{11}B NMR signal, in all probability, due to the low intensity of this signal and overlap with the signal of the borosilicate glass, the NMR tube material.

In order to perform hydroboration of both formate groups, we investigated the reaction of **I** with two molar equivalents of $BH_3{\cdot}SMe_2$. As in the synthesis of **II**, the reaction was carried out in toluene, and crystallization from the solution gave green plate crystals of **III** in 36% yield (Scheme 3); the product was characterized by physicochemical methods, including X-ray diffraction.

The methoxy groups of **III** give single signals, δ_H 2.78 (s, 12H) and δ_C 50.4 (4C) ppm, in the ^{1}H and ^{13}C{^{1}H} NMR spectra, respectively, which attests to equivalence of the four $-OCH_3$ groups in solution. Obviously, this is caused by dynamic processes that are fast on the NMR time scale. It is noteworthy that the chemical shifts characterizing the $-OCH_3$ substituents are similar to those for product **II**. The ^{11}B NMR spectrum does not exhibit signals for the boron atoms that form the six-membered aluminum and boron heterocycle in compound **III** for the same reasons as for **II**. However, the boron atoms of the borohydride anion exhibit a clear-cut ^{11}B{^{1}H} NMR signal at δ_B –41.76 ppm. In addition, the hydride ions of the $[BH_4]^-$ anions give rise to both a septet and quartet at δ_H –0.47 ppm with the ^{1}H–^{10}B ($S(^{10}B) = +3$; J = 27.10 Hz) and ^{1}H–^{11}B ($S(^{11}B) = -3/2$; J = 81.19 Hz) spin–spin coupling constants, respectively.

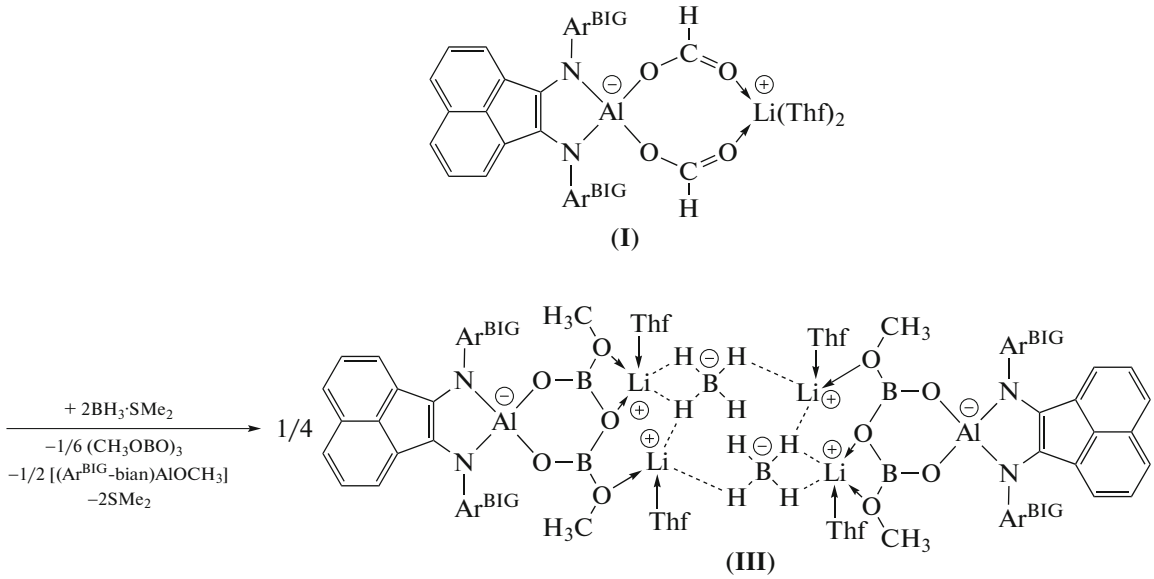

Scheme 3.

As can be seen from Scheme 3, during the formation of compound **III**, both formate groups are reduced to methoxy groups. The relatively low yield of **III** suggests the formation of several reaction products. The most probable scenario describing this process is the initial formation of hydroboration product **II**, which then reacts with the second equivalent of $BH_3{\cdot}SMe_2$. This is followed by a series of intra- and intermolecular reactions accompanied by rearrangements to give not only **III**, but also probably the aluminum derivative [(Ar^{BIG}-bian)AlOCH$_3$] and trimethoxyboroxine $(CH_3OBO)_3$ in 1/4 : 1/2 : 1/6 molar ratio, respectively. To confirm this assumption, we carried out the reaction of **II** with one molar equivalent of borane dimethyl sulfide in THF-d_8 in an NMR tube. Five hours after mixing the reactants, the ^{1}H and ^{11}B{^{1}H} NMR spectra started to exhibit signals for compound **III** and for trimethoxyboroxine, which is characterized by singlets at δ_H 3.47 and δ_B 18.41 ppm [39]. After completion of the reaction (~2 days), the integrated intensity of signals for the methoxy groups in $(CH_3OBO)_3$ and **III** was 1 to 2,

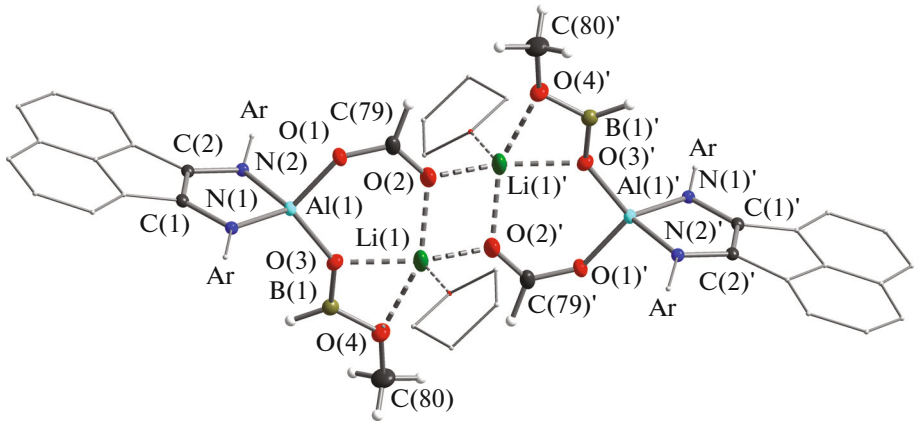

Fig. 1. Molecular structure of complex **II**. Thermal ellipsoids are given at 30% probability level. The hydrogen atoms, except for those bound to C(79), C(80), C(79)', C(80)', B(1), and B(1)' atoms, and 2,6-dibenzhydryl-4-methylphenyl substituents at the nitrogen atoms are not shown.

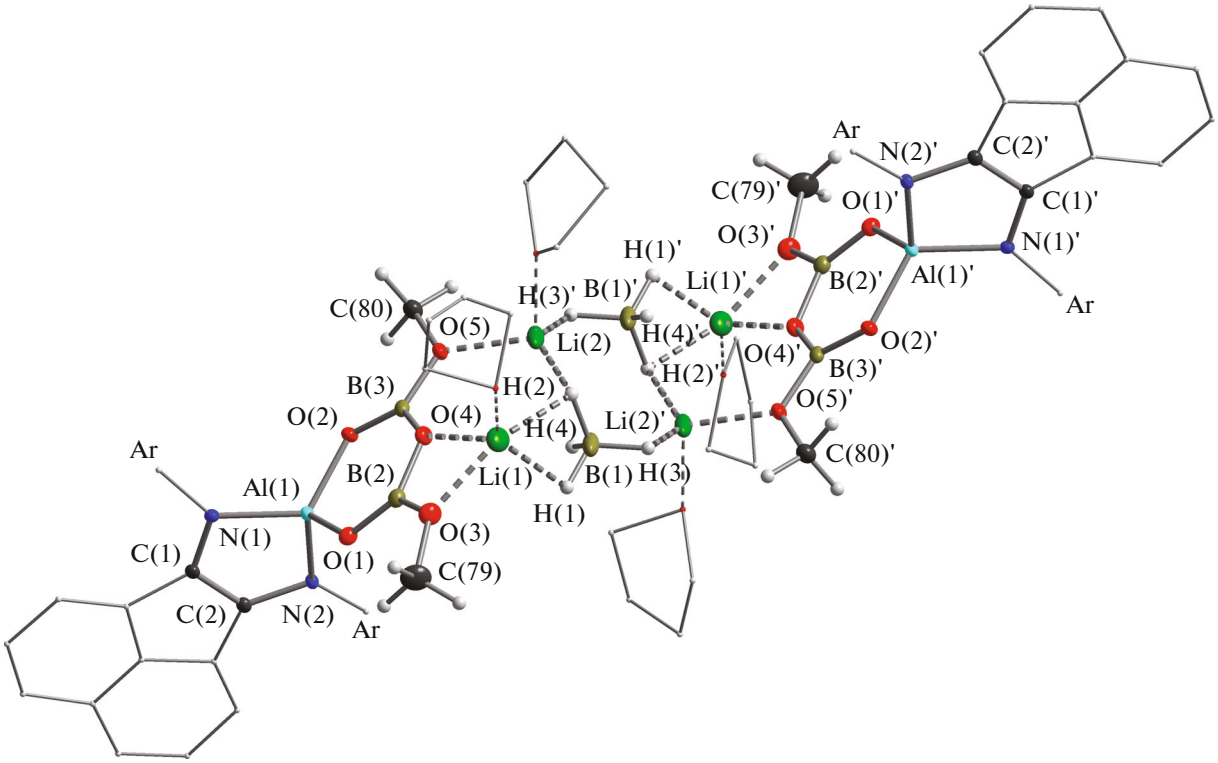

Fig. 2. Molecular structure of complex **III**. Thermal ellipsoids are given at 30% probability level. The hydrogen atoms, except for those bound to C(79), C(80), C(79)', C(80)', B(1), and B(1)' atoms, and 2,6-dibenzhydryl-4-methylphenyl substituents at the nitrogen atoms are not shown.

which corresponds to the molar ratio of these products according to Scheme 3. Unfortunately, we could not identify the hypothesized compound [(Ar^{BIG}-bian)AlOCH$_3$] by NMR spectroscopy, because of the great number of overlapping signals in the regions characteristic of these types of compounds. Repeated attempts to isolate it in a pure crystalline state were also unsuccessful.

The reaction of bis-formate **I** with ammonia was carried out by adding one equivalent of NH_3 by condensation to a frozen solution of **I** in THF. After the reaction mixture was warmed up to room temperature,

the solution color changed from dark blue to green. Green rhombohedral crystals of **IV** were isolated by crystallization (~40 h) from this solution in 70% yield (Scheme 4) and characterized by physicochemical methods of analysis and by X-ray diffraction.

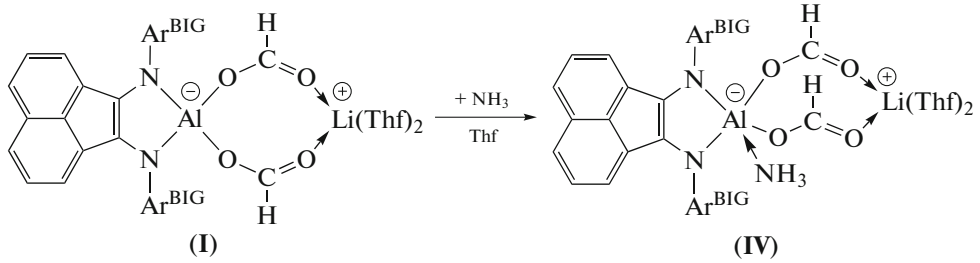

Scheme 4.

This reaction involves neither ammonolysis of Al–N amide bonds nor reaction of ammonia with formate groups of the complex. Instead, one ammonia molecule is coordinated to the metal center. According to ^{1}H NMR data, both formate protons of **IV** are equivalent in solution, giving rise to a singlet at δ_H 6.71 ppm (2H, OC(H)O). The carbon atoms of the OC(H)O groups are characterized by the $^{13}C\{^{1}H\}$ NMR signal at δ_C 166.9 ppm. It should be noted that NH_3 coordination to aluminum induces a 0.27 ppm downfield shift of the proton signal of the formate groups relative to that in **I**. Hydrogen atoms of the ammonia molecule resonate as a broadened singlet at δ_H 0.97 ppm (3H). Also, the chemical shift of the nitrogen atom in the coordinated NH_3 molecule, δ_N 11.5 ppm, was determined by the $^{1}H-^{15}N$ HSQC NMR experiment.

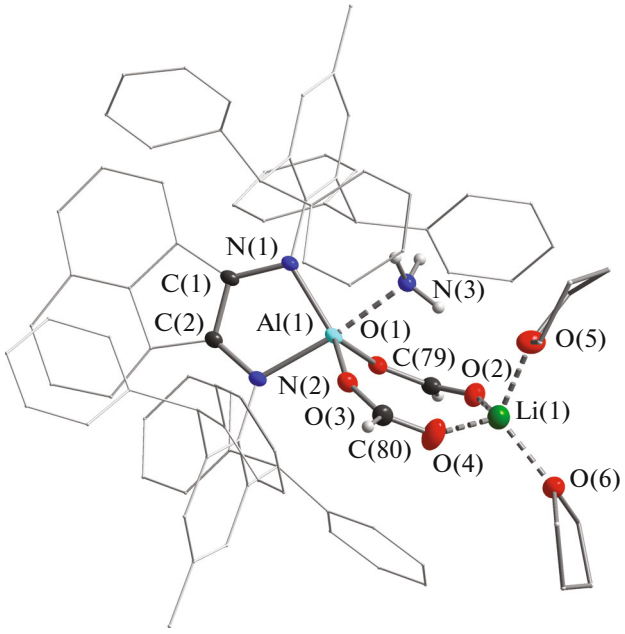

Fig. 3. Molecular structure of complex **IV**. Thermal ellipsoids are given at 30% probability level. The hydrogen atoms, except for those bound to N(3), C(79), and C(80) atoms, are not shown.

The structures of compounds **II**, **III**, and **IV** were established by X-ray diffraction. The molecular structures of complexes **II, III**, and **IV** are shown in Figs. 1, 2, and 3, respectively.

Complex **II** is a centrosymmetric dimer. The inversion center is located in the middle of a planar four-membered metallacycle Li(1)O(2)Li(1)'O(2)'. The formation of dimeric structure **II** is due to the coordination of lithium atoms Li(1) and Li(1)' to bridging oxygen atoms O(2) and O(2)' of two symmetrical formate ligands. In molecule **II**, the formate and methoxyboroxine substituents are tridentate bridging ligands with different coordination modes. The MeOB(H)O ligand binds aluminum and lithium atoms, being coordinated in the μ_2-κO:κ^2O,O' mode. The formate OC(H)O ligand, which binds three metal atoms, has the μ_3-κO:κ^2O' coordination mode [40, 41].

The monomeric moieties of dimer **II** are crystallographically equivalent; therefore, we will discuss the geometric parameters of one of them. The ligand environment of the Al(1) aluminum atom has a distorted tetrahedral geometry (geometric index $\tau_4 = 0.86$) [42], and the environment of the five-coordinate lithium Li(1) atom is close to square pyramid (geometric index $\tau_5 = 0.09$). The Al(1)–O(1), O(1)–C(79), and O(2)–C(79) interatomic distances of the OC(H)O group in **II** differ slightly from those in the initial complex **I** [25] and amount to 1.7972(17), 1.272(3), and 1.218(3) Å, respectively (Table 2). The O(2)–C(79) distance (1.218(3) Å) is typical of a double bond. According to published data, there is only one example of a compound known to date with the $OB(H)OCH_3$ moiety bound to an aluminum atom, namely, the aluminum diketiminate complex (NacNac)Al(Et)$OB(H)OCH_3$ [21]. In **II**, like in the diketiminate derivative, the boron atom has a trigonal geometry. Despite the fact that the lengths of analogous bonds in the $OB(H)OCH_3$ moieties of (NacNac)Al(Et)$OB(H)OCH_3$ and of **II** are similar, in the latter case, the

O(3)–B(1) and B(1)–O(4) interatomic distances are virtually equal (1.347(3) and 1.353(3) Å, respectively) due to lithium coordination. Meanwhile, in the diketiminate derivative [21], these bonds are 1.318(2) and 1.357(3) Å long.

Like complex **II**, compound **III** is a centrosymmetric dimer with the center of inversion located on the line connecting the Li(2) and Li(2)' atoms. In this case, dimerization is due to non-covalent interactions of hydride ions of the borohydride moieties with lithium ions. Each BH_4 group forms Li(1)–H(2)–Li(2) and Li(1)'–H(2)'–Li(2)' μ_3^2 type bridges, whereas the Li(1)–H(1), Li(1)'–H(1)', Li(2)–H(3)', and Li(2)'–H(3) bridges have the μ_2^1 type of binding [43]. Overall, the B(1), H(2), Li(2), H(3)', B(1)', H(2)', Li(2)', and H(3) atoms form an eight-membered cyclic structure, resulting in the formation of dimer **III**. Due to the crystallographic equivalence of the monomeric parts of **III**, the subsequent discussion of the geometrical parameters is given for only one of them. In addition to interactions with borohydride groups, lithium atoms form Li(1)–O(3), Li(1)–O(4), and Li(2)–O(5) coordination bonds with the oxygen atoms of the dimethoxyboroxine unit $(OBOCH_3)_2O$ and with THF oxygen atoms. The Li(1) atom is five-coordinate, with its ligand environment being a distorted tetragonal pyramid (geometric index $\tau_5 = 0.16$). The coordination environment of the Li(2) atom is a distorted tetrahedron (geometric index $\tau_4 = 0.75$). The spiro-centered aluminum atom (C.N. 4) is coordinated to dianionic Ar^{BIG}-bian ligand and to the dimethoxyboroxine unit. The Al(1)–O(1) and Al(1)–O(2) bond lengths in **III** (1.772(3) and 1.756(3) Å, respectively, Table 3) are virtually equal to the Al–O bond lengths (average 1.763 Å) in the starting compound **I** [25]. The AlB_2O_3 ring is planar, as indicated by the sum of ring angles, which is 719.54°, i.e., actually equal (within the error) to the sum of angles of a planar hexagon (720°). The arrangement of the Al(1)–N(1)–C(1)–C(2)–N(2) and Al(1)–O(1)–B(2)–O(4)–B(3)–O(2) rings is nearly orthogonal (89.3°). To date, several NacNac derivatives containing the AlB_2O_3 ring are known [44–47]; however, a complex based on acenaphthene-1,2-dimino ligand with this moiety was obtained for the first time.

Compound **IV** is a product of coordination of the ammonia molecule to bis-formate **I**; as a result, the aluminum atom is five-coordinate, while its ligand environment acquires an intermediate geometry between tetragonal pyramid and trigonal bipyramid (geometric index $\tau_5 = 0.54$).

The increase in the aluminum coordination number leads to some elongation of the Al–N (average 1.907 Å) and Al–O (average 1.835 Å) bonds (Table 4) relative to those in **I**, in which analogous distances are 1.843 Å (average) and 1.763 Å (average), respectively [25]. The N(2), Al(1), and N(3) atoms are virtually in one straight line (the N(2)–Al(1)–N(3) angle is 170°). The Li(1) atom is additionally coordinated by two THF molecules and has a distorted tetrahedral environment ($\tau_4 = 0.91$). In all complexes **II**–**IV**, the N(1)–C(1), C(1)–C(2), and N(2)–C(2) bond lengths are close to one another and are characteristic of the Ar^{BIG}-bian dianion.

Thus, we have accomplished the selective hydroboration of bis-formate complex **I** by borane dimethyl sulfide in 1 : 1 and 1 : 2 molar ratios. This gave monohydroboration product **II** in the former case and a mixture of **III**, trimethoxyboroxine, and presumably complex $[(Ar^{BIG}\text{-bian})AlOCH_3]$ in the latter case. The observed hydroboration products differ from the products of reduction of **I** by pinacolborane [26]. The formation of a high yield of ammonia adduct **IV**, which does not lead to ammonolysis of key bonds in **I**, makes it possible to consider this type of reactions as promising for hydroformylation of amines with carbon dioxide using main group metal acenaphthene-1,2-diimine derivatives as starting compounds.

FUNDING

This study was supported by the Russian Science Foundation no. 20-13-00052 (https://rscf.ru/project/20-13-00052/) and performed using research equipment of the Center for Collective Use "Analytical Center of the Razuvaev Institute of Organometallic Chemistry, Russian Academy of Sciences" supported by the grant "Provision of the Development of Material and Technical Infrastructure of Centers for Collective Use of Research Equipment" (unique identifier RF–2296.61321X0017, agreement number 075-15-2021-670).

CONFLICT OF INTEREST

The authors of this work declare that they have no conflicts of interest.

REFERENCES

1. Lamb, W.F., Wiedmann, T., Pongratz, J., et al., *Environ. Res. Lett.*, 2021, vol. 16, p. 073005.
2. Liu, Q., Wu, L., Jackstell, R., et al., *Nat. Commun.*, 2015, vol. 6, p. 5933.
3. Wang, W.-H., Himeda, Y., Muckerman, J.T., et al., *Chem. Rev.*, 2015, vol. 115, no. 23, p. 12936.
4. Wang, W.-H., Feng, X., and Bao, M., *Transformation of Carbon Dioxide to Formic Acid and Methanol*, Springer Briefs in Molecular Science, Springer Nature, Switzerland AG, 2018.
5. Ye, R.-P., Ding, J., Gong, W., et al., *Nat. Commun.*, 2019, vol. 10, p. 5698.
6. Zhang, Y., Zhang, T., and Das, S., *Green Chem.*, 2020, vol. 22, p. 1800.
7. Ren, M., Zhang, Y., Wang, X., et al., *Catalysts*, 2022, vol. 12, p. 403.

8. Navarro, M., Sánchez-Barba, L.F., Garcés, A., et al., *Catal. Sci. Technol.*, 2020, vol. 10, p. 3265.
9. Laiwattanapaisarn, N., Virachotikul, A., and Phomphrai, K., *Dalton Trans.*, 2021, vol. 50, p. 11039.
10. Yepes, Y.R., Mesías-Salazar, Á., Becerra, A., et al., *Organometallics*, 2021, vol. 40, p. 2859.
11. Saltarini, S., Villegas-Escobar, N., Martínez, J., et al., *Inorg. Chem.*, 2021, vol. 60, p. 1172.
12. Rauch, M. and Parkin, G., *J. Am. Chem. Soc.*, 2017, vol. 139, p. 18162.
13. Rauch, M., Strater, Z., and Parkin, G., *J. Am. Chem. Soc.*, 2019, vol. 141, p. 17754.
14. Huang, W., Roisnel, T., Dorcet, V., et al., *Organometallics*, 2020, vol. 39, p. 698.
15. Caise, A., Hicks, J., Fuentes, M.A., et al., *Chem.-Eur. J.*, 2021, vol. 27, p. 2138.
16. Anker, M.D., Arrowsmith, M., Bellham, P., et al., *Chem. Sci.*, 2014, vol. 5, p. 2826.
17. Yan, B., Dutta, S., Ma, X., et al., *Dalton Trans.*, 2022, vol. 51, p. 6756.
18. Abdalla, J.A.B., Riddlestone, I.M., Tirfoin, R., et al., *Angew. Chem., Int. Ed. Engl.*, 2015, vol. 54, p. 5098.
19. Franz, D., Jandl, C., Stark, C., et al., *ChemCatChem*, 2019, vol. 11, p. 5275.
20. Chia, C.-C., Teo, Y.-C., Cham, N., et al., *Inorg. Chem.*, 2021, vol. 60, p. 4569.
21. Caise, A., Jones, D., Kolychev, E.L., et al., *Chem.-Eur. J.*, 2018, vol. 24, p. 13624.
22. Sokolov, V.G., Koptseva, T.S., Moskalev, M.V., et al., *Russ. Chem. Bull.*, 2017, vol. 66, no. 9, p. 1569. https://doi.org/10.1007/s11172-017-1926-1
23. Moskalev, M.V., Razborov, D.A., Bazanov, A.A., et al., M*endeleev Commun.*, 2020, vol. 30, p. 94.
24. Koptseva, T.S., Moskalev, M.V., Skatova, A.A., et al., *Inorg. Chem.*, 2022, vol. 61, p. 206.
25. Moskalev, M.V., Sokolov, V.G., Koptseva, T.S., et al., *J. Organomet. Chem.*, 2021, vol. 949, p. 121972.
26. Koptseva, T.S., Moskalev, M.V., Skatova, A.A., et al., *Russ. Chem. Bull.*, 2022, vol. 71, no. 8, p. 1626. https://doi.org/10.1007/s11172-022-3571-6
27. Koptseva, T.S., Skatova, A.A., Ketkov, S.Y., et al., *Organometallics*, 2023, vol. 42, p. 123.
28. Guzmán, J., Torguet, A., García-Orduña, P., et al., *J. Organomet. Chem.*, 2019, vol. 897, p. 50.
29. Li, Z., Yu, Z., Luo, X., et al., *RSC Adv.*, 2020, vol. 10, p. 33972.
30. Lin, S., Liu, J., and Ma, L., *J. CO2 Util.*, 2021, vol. 54, p. 101759.
31. Zhai, G., Liu, Q., Ji, J., et al., *J. CO2 Util.*, 2022, vol. 61, p. 102052.
32. *APEX3. Bruker Molecular Analysis Research Tool. Version 2018.7-2*, Madison: Bruker AXS Inc., 2018.
33. *SAINT. Data Reduction and Correction Program. Version 8.38A*, Madison: Bruker AXS Inc., 2017.
34. Krause, L., Herbst-Irmer, R., Sheldrick, G.M., and Stalke, D., *J. Appl. Crystallogr.*, 2015, vol. 48, p. 3.
35. Sheldrick, G.M., *Acta Crystallogr., Sect. A: Found. Adv.*, 2015, vol. 71, p. 3.
36. Sheldrick, G.M., *SHELXTL. Version 6.14. Structure Determination Software Suite*, Madison: Bruker AXS, 2003.
37. Sheldrick, G.M., *Acta Crystallogr., Sect. C: Struct. Chem.*, 2015, vol. 71, p. 3.
38. Sheldrick, G.M., *SADABS. Version 2016/2. Bruker/Siemens Area Detector Absorption Correction Program*, Madison: Bruker AXS, 2016.
39. Leong, B.-X., Lee, J., Li, Y., et al., *J. Am. Chem. Soc.*, 2019, vol. 141, p. 17629.
40. Saxena, P. and Thirupathi, N., *Polyhedron*, 2015, vol. 98, p. 238.
41. Lago, A.B., Carballo, R., Lezama, L., et al., *J. Solid State Chem.*, 2015, vol. 231, p. 145.
42. Yang, L., Powell, D.R., and Houser, R.P., *Dalton Trans.*, 2007, p. 955.
43. Ruiz, J.C.G., Nöth, H., and Warchhold, M., *Eur. J. Inorg. Chem.*, 2008, p. 251.
44. Yang, Z., Ma, X., Oswald, R.B., et al., *J. Am. Chem. Soc.*, 2006, vol. 128, p. 12406.
45. Ma, X., Yang, Z., Wang, X., et al., *Inorg. Chem.*, 2011, vol. 50, p. 2010.
46. Ma, X., Zhong, M., Liu, Z., et al., *Z. Kristallogr. NCS*, 2012, vol. 227, p. 580.
47. Yang, Z., Hao, P., Liu, Z., et al., *J. Organomet. Chem.*, 2014, vol. 751, p. 788.

Translated by Z. Svitanko